Chinese Chemical Letters 37 (2026) 111798

Contents lists available at ScienceDirect

Chinese Chemical Letters

journal homepage: www.elsevier.com/locate/cclet

"Dual sweet" supramolecular glycosyl-nanoproteins based on carbohydrate-protein interaction for targeted drug delivery *in vivo*

Kun Shang[a,c,1], Yinghua Lv[a,1], Yibo Yang[a,1], Senyu Yang[a], Zelong Chen[a], Ke Yang[a], Cong Li[a], Shuang Chao[a,*], Yuchao Lu[b,*], Yuxin Pei[a,*], Zhichao Pei[a,*]

[a] College of Chemistry & Pharmacy, Northwest A&F University, Yangling 712100, China
[b] School of Pharmacy, Changzhi Medical College, Shanxi Provincial Department-Municipal Key Laboratory Cultivation Base for Quality Enhancement and Utilization of Shangdang Chinese Medicinal Materials, Changzhi 046000, China
[c] Yan'an Medical College of Yan'an University, Yan'an 716000, China

ARTICLE INFO

Article history:
Received 24 March 2025
Revised 25 August 2025
Accepted 7 September 2025
Available online 9 September 2025

Keywords:
Carbohydrate-protein interactions
Glycosyl-nanoproteins
Supramolecular self-assembly
Drug-targeted delivery
Chemotherapy

ABSTRACT

Biomolecular self-assembly systems form the cornerstone of biological structures, in which the interactions between carbohydrates and proteins play a crucial role in many life processes. This has driven the development of biomimetic carbohydrate-protein supramolecular assemblies (BCPSAs), which show great potential in biomedical research. We successfully constructed a novel supramolecular hybrid nanocarrier with pH responsiveness and targeting capabilities based on specific interactions between carbohydrates and proteins. This system self-assembles into nanoparticles CA@MP5 in water through the specific binding of mannose clusters on glycosylated pillar[5]arene MP5 with lectin Con A. Additionally, through a host-guest assembly strategy with the synthesized β-D-galactopyranosyl pyridine derivative G, it complexes within the MP5 cavity to form a "double-sweet" supramolecular glyco-nanoprotein (CA@MP5⊃G). This system shows high affinity for the asialoglycoprotein receptor (ASGPR) on HepG2 liver cancer cells. *In vitro*, the doxorubicin (DOX)-loaded micelles (DCA@MP5⊃G) release drug effectively in acidic environments and significantly inhibit HepG2 cell growth, with reduced toxicity toward normal cells. *In vivo*, the nanocarrier targets tumors effectively, reducing systemic toxicity and inhibiting tumor growth. This study offers a novel construction strategy for drug delivery systems based on carbohydrate-protein interactions in anti-tumor applications, which is significant for enhancing therapeutic efficacy.

© 2026 Published by Elsevier B.V. on behalf of Chinese Chemical Society and Institute of Materia Medica, Chinese Academy of Medical Sciences.

The foundation of biological structures is based on the self-assembly systems of biomolecules, which lead to the formation of numerous highly complex and dynamically changing structures [1–3]. Among these, specific structures resulting from carbohydrate-protein interactions play a crucial role in the life activities of plants, animals, and microorganisms [4–7]. These structures are extensively involved in intercellular communication and signal transduction, regulating cell adhesion, migration, and proliferation, while also deeply participating in pathogen recognition and the modulation of immune responses [8–11]. Inspired by this, researchers have developed dynamic, controllable supramolecular assemblies based on carbohydrates, that containing a large amount of proteins, known as biomimetic carbohydrate-protein supramolecular assemblies (BCPSAs) [12–17]. These BCPSAs typically exhibit excellent biocompatibility and mimic the structure and function of natural proteins in biological systems, allowing them to better simulate the physiological environment and biological processes within organisms [18–21]. Consequently, BCPSAs have become ideal model systems in biomedical research, with wide applications in studying intercellular interactions, signal transduction mechanisms, and disease development processes, as well as showing great potential in drug delivery, bioimaging, and medical tissue engineering.

In recent years, a variety of glyco-conjugates using macrocyclic molecules as the core for coupling carbohydrates have been reported [22,23]. Compared to monosaccharides, glycoclusters can exhibit polyvalent carbohydrate-protein receptor interactions similar to glycans [24,25]. This multivalent effect greatly enhances the specificity and affinity of recognition, allowing for more precise targeting of molecules in biological recognition processes, whether in cell surface receptor recognition or biomolecular detection [26,27]. Additionally, macrocyclic molecules possess stable structures and specific cavities, enabling them to form dynamic

* Corresponding authors.
E-mail addresses: chaoshuang@nwafu.edu.cn (S. Chao), luyuchao@czmc.edu.cn (Y. Lu), peiyx@nwafu.edu.cn (Y. Pei), peizc@nwafu.edu.cn (Z. Pei).
[1] These authors contributed equally to this work.

https://doi.org/10.1016/j.cclet.2025.111798
1001-8417/© 2026 Published by Elsevier B.V. on behalf of Chinese Chemical Society and Institute of Materia Medica, Chinese Academy of Medical Sciences.

and precise host-guest assemblies with various guest molecules through hydrogen bonding, electrostatic interactions, π-π stacking, ion-π interactions, hydrophobic effects, coordination, and halogen bonding [28–31]. This provides significant advantages in achieving multifunctionality in BCPSA systems. Moreover, glycoclusters have well-defined molecular structures that can be easily adjusted dynamically for targeted functions, laying a foundation for constructing functionally tunable biomimetic BCPSAs.

Pillararenes, as a representative of a new generation of supramolecular macrocyclic hosts, have attracted significant attention due to their easily modifiable side chains, symmetrical electron-rich cavities, and stable rigid frameworks [32–37]. In the design and synthesis of glycoclusters using macrocyclic molecules as the core framework, pillararenes demonstrate unique advantages, which can more easily conjugate multiple sugar molecules [38–41]. This is primarily because pillararenes can achieve the conjugation of multiple sugar molecules at both ends without the need for new scaffold extension binding sites. Furthermore, the structure of pillararenes simplifies and enhances flexibility in functional modification, allowing adaptation to different reaction conditions for conjugating sugar and other functional molecules [42–44]. These advantages make glycosylated pillararenes crucial in constructing BCPSAs with functions like biological recognition and drug delivery.

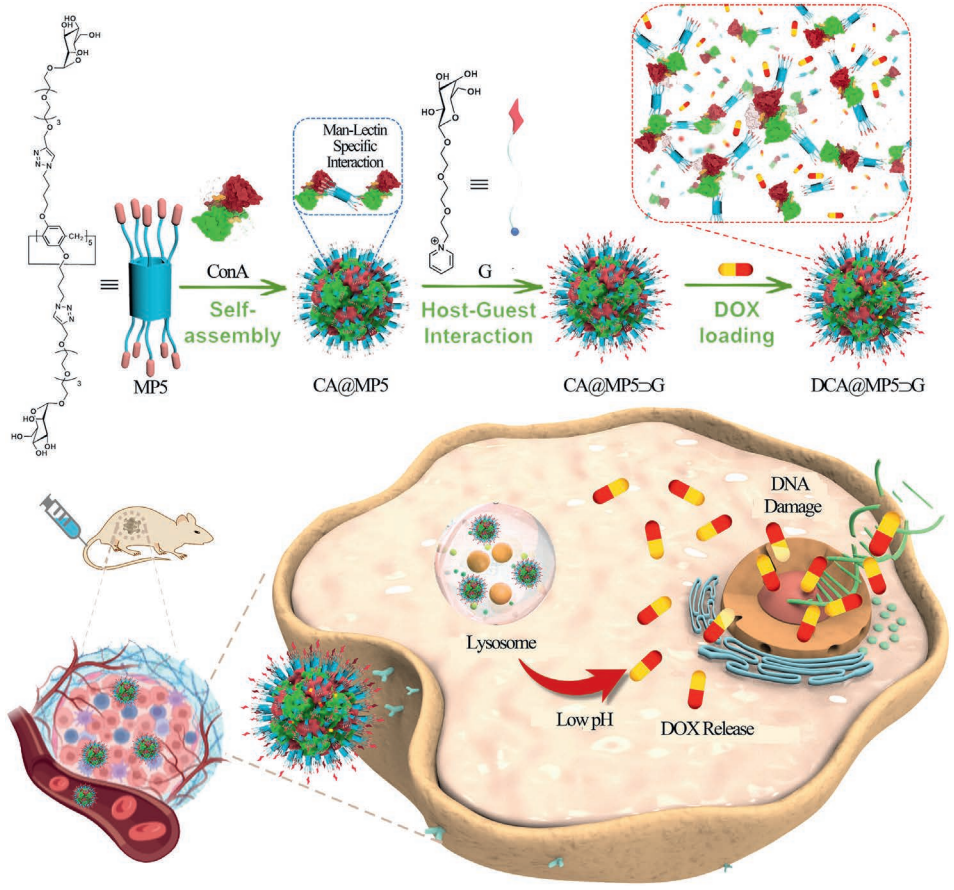
In this study, we utilized carbohydrate-protein interactions to construct a supramolecular biohybrid nanomicelle system through a modular approach for drug targeted delivery. This system relies on the multivalent effect of glycosylated pillararenes, particularly the specific binding between mannose-modified pillar[5]arenes (MP5) and the lectin Con A, resulting in the formation of structurally stable and biocompatible BCPSAs Con A@MP5 (CA@MP5). The MP5 modified mannose cluster mainly serves as a skeleton, and its core function is to drive the self-assembly of CA@MP5 nanoparticles through the sugar protein specific interaction between mannose and lectin Con A, constructing a structurally stable supramolecular carrier skeleton. At the same time, we utilized the dynamic binding characteristics between the MP5 cavity and guest molecules to synthesize pyridine derivatives of β-D-galactose (G) and incorporated them into the cavity of MP5 through host assembly strategy, thereby making the system highly affinity for the overexpression of asialoglycoprotein receptor (ASGPR) on the surface of HepG2 cells (liver cancer cells). Doxorubicin (DOX), a drug widely used in cancer therapy, was selected as a model drug and loaded into the nanoparticles to create “dual sweet” supramolecular glycosyl-nanoproteins DCA@MP5⊃G (Dox-loaded CA@MP5⊃G). When these nanoparticles reach the tumor tissue and enter the liver cancer cells *via* ASGPR-mediated endocytosis, the low pH environment in the lysosomes reduces the interaction between Con A and MP5, prompting the disassembly of the nanoparticles and the release of DOX. This mechanism enables targeted drug delivery and controlled release, significantly enhancing chemotherapy efficacy while effectively reducing side effects on normal tissues. This system ingeniously utilizes glycosyl macrocycles as efficient modules, showcasing their unique advantages in the construction of BCPSAs. It fully highlights the core role of carbohydrate-protein interactions in biological recognition and targeted therapy, offering new insights and practical examples for the field of nanomedicine.

Firstly, we synthesized alkynyl-functionalized peracetylated mannose by referring to the method previously reported by our group, and then connected it with azido-functionalized pillararene through a click reaction to obtain peracetylated mannosyl pillar[5]arene. After deacetylation, the mannose-functionalized pillar[5]arene MP5 was obtained. Meanwhile, the guest molecule, pyridyl-modified galactose as a targeting molecule, was synthesized by referring to the synthetic method previously reported by our group. Please refer to Schemes S1 and S2, and Figs. S1–S10 (Supporting information) for the specific synthesis steps and structural characterizations of MP5 and G.

The schematic illustration of the preparation of CA@MP5⊃G is presented in Scheme 1. Initially, the interaction between Con A and MP5 was investigated by circular dichroism (CD) spectroscopy. As depicted in Fig. 1a, upon the addition of varying concentrations of MP5, the absorbance of Con A at 220 nm progressively diminished. Notably, when the molar ratio of Con A to MP5 reached 2:7, an equilibrium was attained, and the absorbance of Con A ceased to vary with further increments in MP5 concentration. Consequently, a Con A:MP5 ratio of 2:7 was chosen for the fabrication of the CA@MP5 supramolecular nanoprotein assembly. Subsequently, the critical micelle concentration of CA@MP5 was determined to be 25.40 μmol/L using the interface tension meter (Fig. 1b). The pyridyl galactose derivative G was designed and synthesized then modified onto CA@MP5 as a guest molecule to achieve targeted delivery of the nanoprotein assembly to liver cancer cell lines overexpressing ASGPR. The assembly of G with MP5 at different ratios was determined by ultraviolet titration (Fig. S11 in Supporting information), and a Job plot curve was generated using the absorbance of MP5 at 295 nm (Fig. 1c). The results indicated that the optimal complexation ratio of G to MP5 was 1:1. Subsequently, G was added to the CA@MP5 solution to prepare CA@MP5⊃G. The dynamic light scattering (DLS) results showed that the average hydrodynamic radius of CA@MP5⊃G was approximately 214.79 ± 4.69 nm (Fig. 1d). Meanwhile, the scanning electron microscopy (SEM) and transmission electron microscopy (TEM) observations revealed that the CA@MP5⊃G nanoparticles were spherical nanomicelles (Figs. 1e and f). These results demonstrated that the CA@MP5⊃G BCPSAs were successfully prepared.

The anticancer drug DOX was loaded into CA@MP5⊃G as a model drug to prepare DCA@MP5⊃G. The DLS test results showed that the diameter of the nanoparticles was 189.36 ± 2.93 nm (Fig. 2a). This size is slightly smaller than that of CA@MP5⊃G, mainly because the DOX in DCA@MP5⊃G aggregates with MP5 or Con A through π-π interaction or hydrophobic interaction, thus changing the size of the nanoparticles. DCA@MP5⊃G also has good dispersibility in water and exhibits an obvious Tyndall effect (Fig. S12 in Supporting information). The SEM observation results showed that DCA@MP5⊃G is still spherical (Fig. 2b). Meanwhile, the encapsulation efficiency and loading rate of DCA@MP5⊃G for DOX are 81.1 % and 56.7 %, respectively. These results all prove that DCA@MP5⊃G can be an effective carrier for drugs. Meanwhile, stability tests demonstrated that DCA@MP5⊃G maintained its hydrodynamic diameter in PBS (pH 7.4) over 5 days, with almost no change in particle size, indicating good stability (Fig. S13 in Supporting information).

The pH value in the microenvironment of cancer cells is lower than that of normal cells. We use acidic buffers to simulate the acidic microenvironment of cancer cells to test the pH-responsive release effect of the supramolecular hybrid nanosystem CA@MP5⊃G. According to the UV absorption curve of DOX at 488 nm, we calculated the DOX release at different time. The release profiles of DCA@MP5⊃G were investigated by using PBS with different pH values as the release medium through the dialysis method. As shown in the Fig. 2c, in the neutral environment the same as normal cells are located, the hybrid nanosystem CA@MP5⊃G was very stable, and only a small amount of drug leakage occurred. However, under neutral conditions, the final nanomicelles release only a small amount of DOX; and the release of a large amount of drug DOX is triggered in the acidic microenvironment, indicating that the hybrid nanosystem has good pH responsiveness, which is due to depolymerization of Con A under acidic conditions. It further leads to the disintegration of the supramolecular hybrid nanosystem CA@MP5⊃G. The observation results of SEM also indicate that the nanoparticles depolymerize



Scheme 1. Schematic illustration of "dual sweet" supramolecular glycosyl-nanoproteins based on carbohydrate-protein interaction for targeted drug delivery *in vivo*.

in a low pH environment (Fig. 2d). The characteristics of the responsive release of drugs in the acidic microenvironment indicate that CA@MP5⊃G is expected to become an excellent supramolecular hybrid nanosystem that reduces the toxicity of drugs to normal cells.

As we know that ASGPRs overexpressed on the HepG2 cell membrane surface can specifically recognize galactose residues. The guest of galactose in this system is expected to have the ability to specifically recognize ASGPRs. In order to evaluate the targeting ability of the hybrid system nanomicelles to the HepG2 cell which overexpressing ASGPRs on the cell membrane surface, we incubated the medium containing free DOX or DOX-encapsulated nanomicelles with 293T cells (human embryonic kidney T) or HepG2 cells for 4 h. One group was pre-incubated with lactobionic acid (LA, 2 mg/mL) before adding the nanomicelles. The DOX fluorescence in the cells of each test group was obtained through the fluorescence channel of the laser scanning confocal microscope to directly observe the targeting effect of the supramolecular hybrid system. As shown in the Figs. 3a and b, we found that the fluorescence is the most obvious in HepG2 cells relatively (G3), and the result is significantly better than the free DOX group during the same period. At the same time, there is only weak fluorescence in 293T cells treated with DOX-loaded nanomicelles. In addition, when the HepG2 cells were pretreated with LA, the uptake of the DOX-loaded micelles by the HepG2 cells in this group was significantly reduced.

In order to further verify the targeting effect of the hybrid system, we used flow cytometry to analyze each group of cells with the same treatment. As shown in the Fig. 3c, the DOX-loaded nanomicelles were more taken up by the third group of HepG2 cells, and the results were similar to those observed in CLSM. These studies show that the presence of the galactose on the surface of the hybrid system was very important. If the galactose residues in lactobionic acid occupy the galactose receptor of ASGPRs on the surface of HepG2 cells, it will hinder the recognition of the hybrid system with HepG2 cells, and ultimately hinder the ASGPRs-mediated cellular uptake. Overall, ASGPRs overexpressed on the membrane surface of HepG2 cells play an important role in the cellular uptake of DOX-loaded nanomicelles. It increased the endocytosis of the cell uptake of drugs, and receptor-mediated endocytosis relatively increased the intake of cells to the DOX-loaded hybrid system. The hybrid nanosystem can achieve targeted drug delivery to HepG2 cells through ASGPRs-mediated endocytosis.

After the preliminary preparation of the experiment, we ultrasonicated the mixed solution of DOX and nanomicelles, and then the mixture was stood and dialyzed to obtain the DOX-loaded nanomicelles, which morphology was observed. The annexin V conjugate staining assay was used to evaluate the killing effect of DOX and DOX-loaded nanomicelles on HepG2 cells. As shown in Figs. 4a–d, after the treatment of HepG2 cells 24 h by the DOX-loaded nanomicelles, while the free DOX caused only a small amount of early apoptosis of HepG2 cells, the DOX-loaded nanomicelles had already caused nearly half of the HepG2 cells to undergo apoptosis or necrosis. The hybrid nano-micelles greatly improved the apoptosis-promoting effect of the drug. To further validate the *in vitro* cell killing effect of DCA@MP5⊃G, we performed fluorescence staining of live/dead cells, and the results after 24 h of treatment in different treatment groups are shown in Fig. S14 (Supporting information). Compared with free DOX which only caused a small amount of early apoptosis, DCA@MP5 had caused apopto-

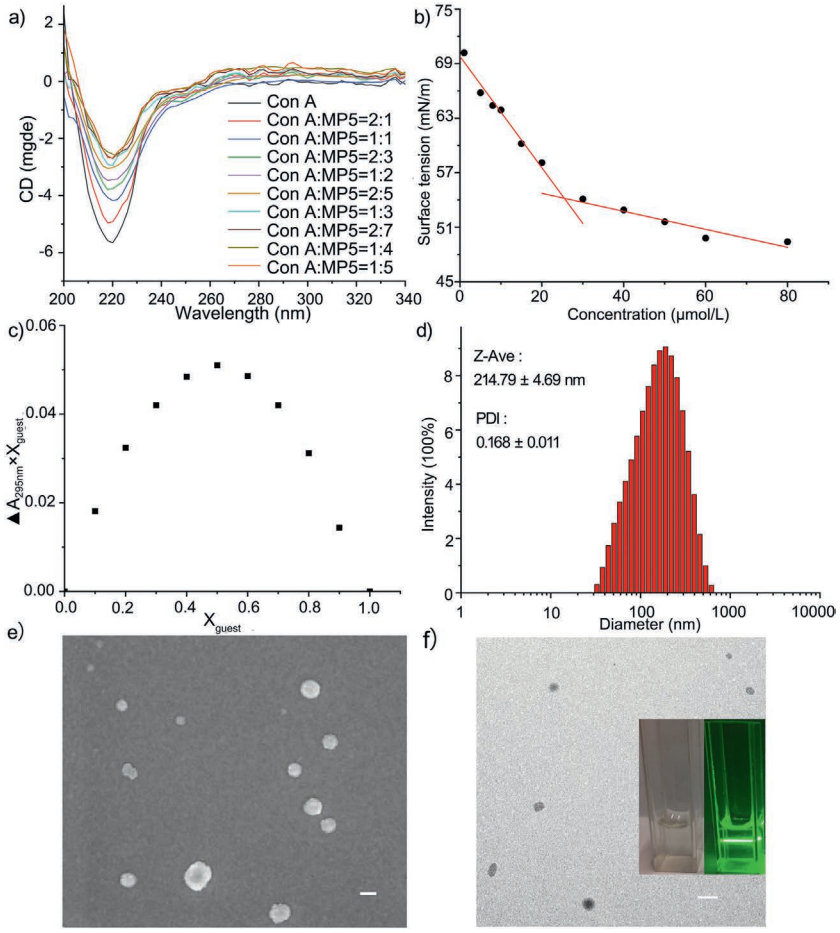


Fig. 1. Preparation and characterization of CA@MP5⊃G. (a) The different ratio of the combination of the MP5 with Con A. (b) The critical micelle concentration of CA@MP5 in water. (c) Job plot of the difference in absorption with MP5 against the G in aqueous solution. (d) DLS analysis of the CA@MP5⊃G. (e) SEM image of CA@MP5⊃G (Scale bar: 100 nm). (f) TEM image of CA@MP5⊃G and Tyndall effect of CA@MP5⊃G. Scale bar: 200 nm.

sis or necrosis in nearly half of the HepG2 cells. Meanwhile, the galactose on the surface of the nanocarrier interacted specifically with the overexpressed ASGPRs, thus facilitating the targeted delivery of the nanomicelles to the hepatocellular carcinoma cells, and DCA@MP5⊃G led to a significant increase in the death of the tumor cells and a significant enhancement of the red fluorescence.

Since the pro-apoptotic effects of DOX and DOX-loaded micelles had been studied, their anti-cancer effects at different times have been explored. To this end, HepG2 cells and 293T cells were incubated with micelles or DOX for 24, 48, and 72 h, respectively. At the end of the treatment, we found that the cell viability of the HepG2 cells treated with the DOX-loaded micelles was significantly lower than that of the HepG2 cells treated with free DOX. At the same time, 293T cells treated with DOX-loaded micelles relatively have higher cell viability than that of the 293T cells treated with free DOX (Figs. 4e and f). The DCA@MP5⊃G micelles could kill the HepG2 cells that were more efficient than the equivalent free DOX. Compared with free DOX, DCA@MP5⊃G could effectively improve the survival of 293T cells. It can be seen that the drug was encapsulated by the supramolecular hybrid nanomicelles increases the killing effect of the drug on cancer cells while greatly reducing the side effects of the drug on normal cells. The above result also proves the rationality and effectiveness of our design on the drug delivery system. By gathering galactose clusters on the surface of the micelles, it produced the glycocluster effect, which increases the specific interaction between the surface of the hybrid nanomicelles and the HepG2 cells with overexpressing ASGPRs, and then promotes the targeted delivery process of nanomicelles to liver cancer cells. In summary, all the results indicate that the nanomicelle is a new type of nano-delivery system with excellent biocompatibility, targeted, controlled release, which is expected to be applied to the treatment of tumors.

Mitochondria play a crucial role in regulating cell proliferation and death. Nanoparticle mediated mitochondrial damage may induce apoptosis in cancer. Normal mitochondrial membrane potential (MMP) maintains mitochondrial biological function. The decrease of MMP is an important index of early apoptosis of tumor cells. In order to explore the tumor cytotoxicity mechanism of DCA@MP5⊃G and explore the effect of drug loaded nanoparticles on the mitochondrial apoptosis pathway. We used a JC-1 probe to detect the MMP in tumor cells. As shown in Fig. 5a, the green fluorescence (JC-1 monomer) in group DCA@MP5⊃G cells were significantly higher than that in DOX alone group and group DCA@MP5, indicating that galactose modified drug loaded nanoparticles can significantly reduce MMP and affect mitochondrial function. The analysis of tumor damage by Western blot also showed that DCA@MP5⊃G strongly activated the guard of genome p53 phosphorylation at Ser 15, thus activating p53 mediated apoptosis, which further upregulated the pro-apoptotic protein BAX and down-regulated the anti-apoptotic protein BCL2 (Fig. 5b). Taken together, these results suggest that our carbohydrate modified pillar[5]arene–lectin supramolecular bio-hybrid nano-loading platform can help enhance the transmission of DOX to tumor cells, thereby reducing MMP, and activating the mitochondria apopto-

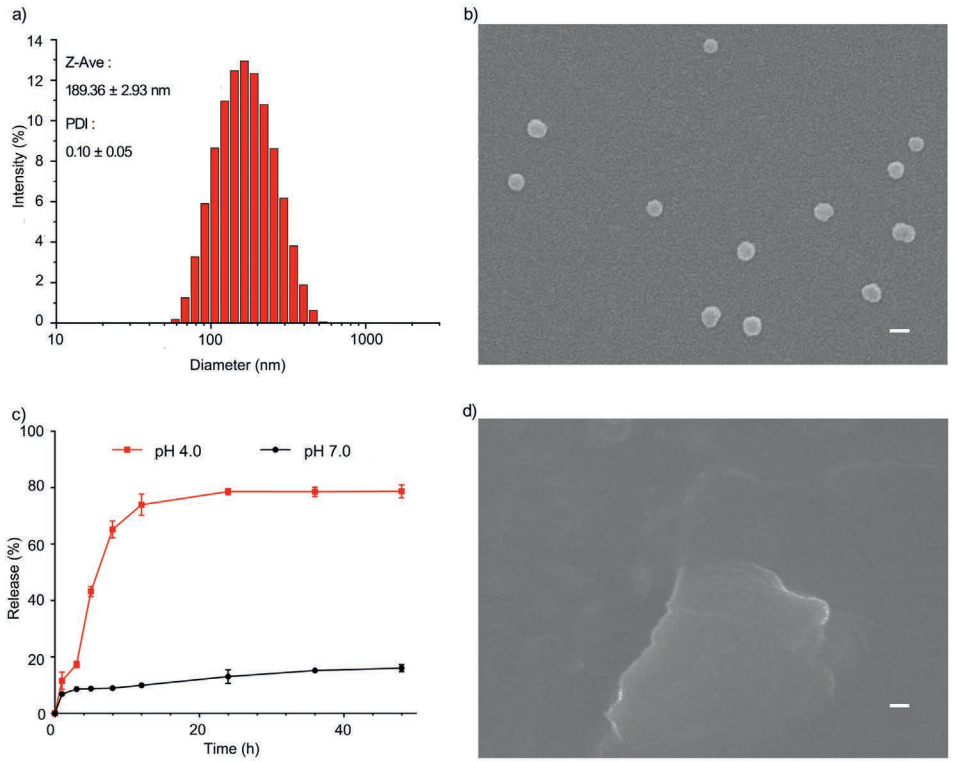


Fig. 2. (a) DLS analysis of the DCA@MP5⊃G. (b) SEM image of the DCA@MP5⊃G. (c) DOX release profiles of DCA@MP5⊃G in neutral and acidic environment. Data are presented as mean ± standard deviation (SD) ($n = 3$). (d) SEM image of CA@MP5⊃G in the acidic environment (pH 4.0). Scale bar: 200 nm.

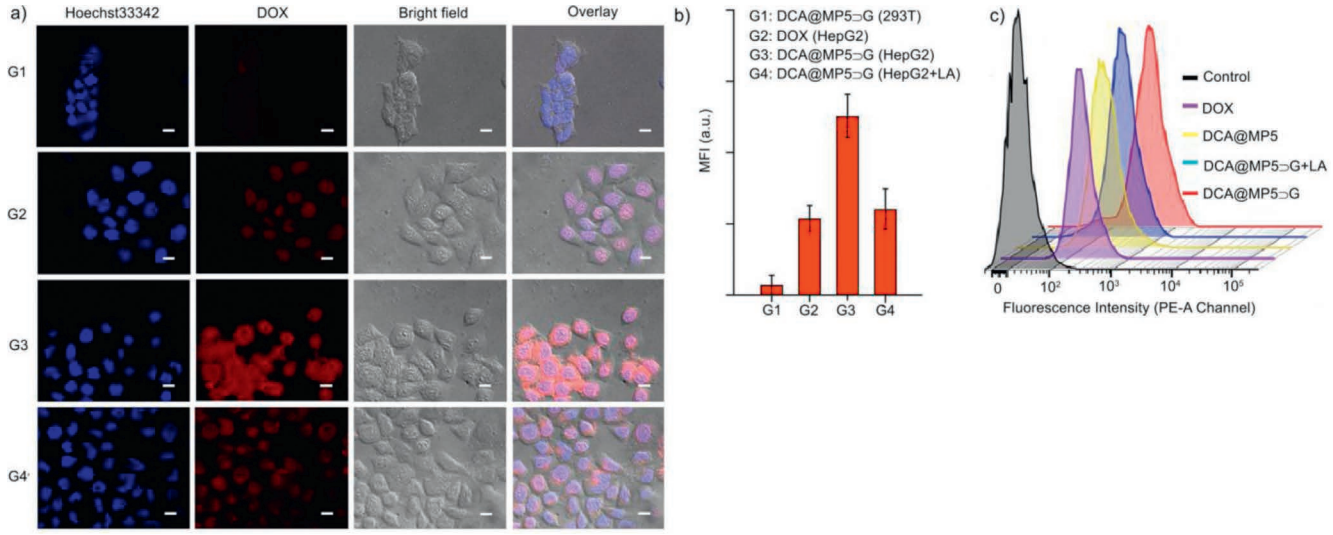


Fig. 3. (a) Confocal laser scanning microscopy (CLSM) images of 293T cells (G1), HepG2 cells (G3) cultured with DCA@MP5⊃G for 4 h. CLSM images of HepG2 cells (G4) cultured with DCA@MP5⊃G for 4 h pre-incubated with LA. CLSM images of HepG2 cells (G2) were cultured with DOX for 4 h. The nuclei were stained with hoechst33342. The scale bar is 5 μm. (b) The corresponding mean fluorescence intensity of DOX in different groups (G1–G4). Data are presented as mean ± standard deviation (SD) ($n = 10$). (c) Flow cytometry analyses of HepG2 cells incubated in free DOX, DCAA@MP5⊃G, or DCA@MP5⊃G after preincubation with LA for 4 h, respectively.

sis signaling pathway, which ultimately induces tumor cell death and markedly enhances the antitumor efficacy of chemotherapeutic drugs.

Over the past few decades, research has indicated that intravenous administration of DOX leads to cumulative, dose-dependent cardiotoxicity, which significantly elevates the risk of mortality. To assess the long-term systemic toxicity of DCA@MP5⊃G, immunodeficient BALB/C athymic nude mice were administered the treatment. All animal care and handling procedures were conducted in compliance with protocols approved by the Animal Care and Use Committee of Northwest A&F University (Shaanxi, China). Following the final treatment, the mice were euthanized, and tumors/organs were collected for *ex vivo* imaging. DOX accumulation was quantified using a PerkinElmer IVIS *in vivo* imaging system [45,46]. As shown in Fig. 6a, the DOX-loaded hybrid nanosystem (DCA@MP5⊃G) demonstrates significantly stronger aggregated fluorescence signals within the tumor tissue, whereas no detectable fluorescence was observed in the naked DOX group and the DCA@MP5 group under the same excitation intensity conditions. Moreover, no significant fluorescence was detected in the

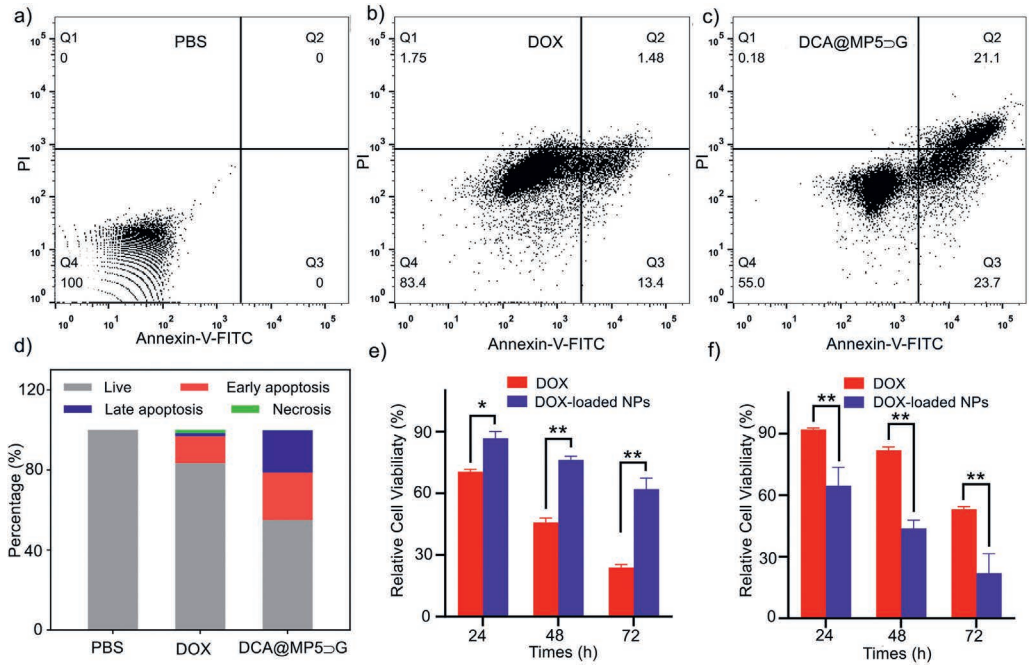


Fig. 4. Cell viability measurement by Annexin V-FITC/PI apoptosis assays and MTT method. (a-c) The Annexin V-FITC/PI apoptosis assay of HepG2 cells with PBS, DOX, DCA@MP5⊃G, respectively. (d) Quantitative analysis of apoptosis-related percentages (gray: Live, red: Early apoptosis, blue: Late apoptosis, green: Necrosis) for HepG2 cells treated with PBS, DOX, and DCA@MP5⊃G, matching the assays in (a-c). The concentration of DOX was 2.0 μmol/L. The toxicity of DOX and DCA@MP5⊃G on (e) 293T cells and (f) HepG2 cells for 24, 48, and 72 h. The concentration of DOX was 1.0 μmol/L. Data are presented as mean ± standard deviation (SD) ($n = 6$). $^{*}P < 0.05$, $^{**}P < 0.001$.

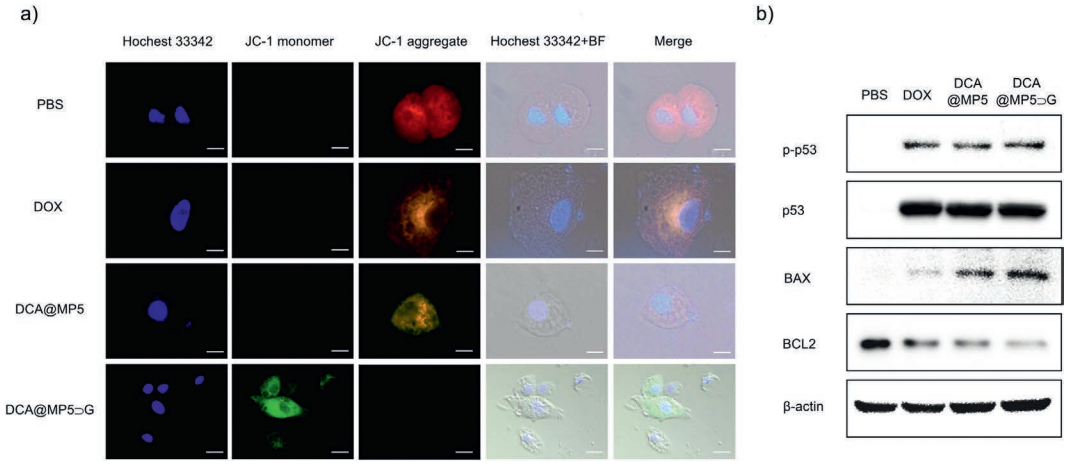


Fig. 5. (a) Fluorescence microscopy images of HepG2 cells stained with JC-1 dye after various treatments for 4 h. Red color indicates high MMP and green color indicates low MMP. The scale bar is 5 μm. (b) Expression of apoptotic markers analyzed by Western blot in HepG2 cells treated with different formulations for 48 h.

heart, liver, spleen, lung, or kidney (Fig. 6b), demonstrating that DOX delivered by DCA@MP5⊃G exhibits distinct tumor-targeting capabilities in the HepG2 tumor model *in vivo*. In addition, the body weight of HepG2 tumor bearing mice in the DOX group exhibited a notable decline (Fig. 6c), indicative of the potential for DOX to exert considerable systemic toxicity. In comparison, the average body weight of nude mice in group DCA@MP5⊃G remained comparable to that in PBS group, suggesting that the carbohydrate modified pillar[5]arene–lectin bio-hybrid nano-loading platform may effectively serve to mitigate the systemic toxicity typically associated with DOX. Additionally, we evaluated the routine blood parameters including red blood cells (RBC), white blood cells (WBC), platelets (PLT), hemoglobin (HGB), and hematocrit (HCT) to further assess the biosafety profile of DCA@MP5⊃G nanoparticles. As shown in Fig. 6d, a deduction of WBC, HCT was observed in the DOX-treated group, while the DCA@MP5⊃G group remained in the normal range. Moreover, the main organs of tumor bearing nude mice, including heart, liver, spleen, lung and kidney were dissected for hematoxylin-eosin (HE) staining to evaluate the *in vivo* safety of DCA@MP5⊃G nano drug delivery system. As shown in Fig. 6e, no obvious pathological changes were observed in group DCA@MP5⊃G compared to the normal PBS group. These findings indicate that the carbohydrate-modified pillar[5]arene-lectin supramolecular bio-hybrid nano-loading platform, which facilitates DOX delivery, exhibits excellent tumor-targeting capabilities and tumor-responsive drug release *in vivo*. This system effectively minimizes the systemic toxicity of DOX while simultaneously improving its anti-tumor therapeutic potential.

To further assess the tumor-inhibitory efficacy of DCA@MP5⊃G, HepG2-bearing BALB/c nude mice were randomly allocated into four groups: (1) PBS (control), (2) DOX, (3) DCA@MP5, and (4) DCA@MP5⊃G. The drug was administered *via* tail vein injection

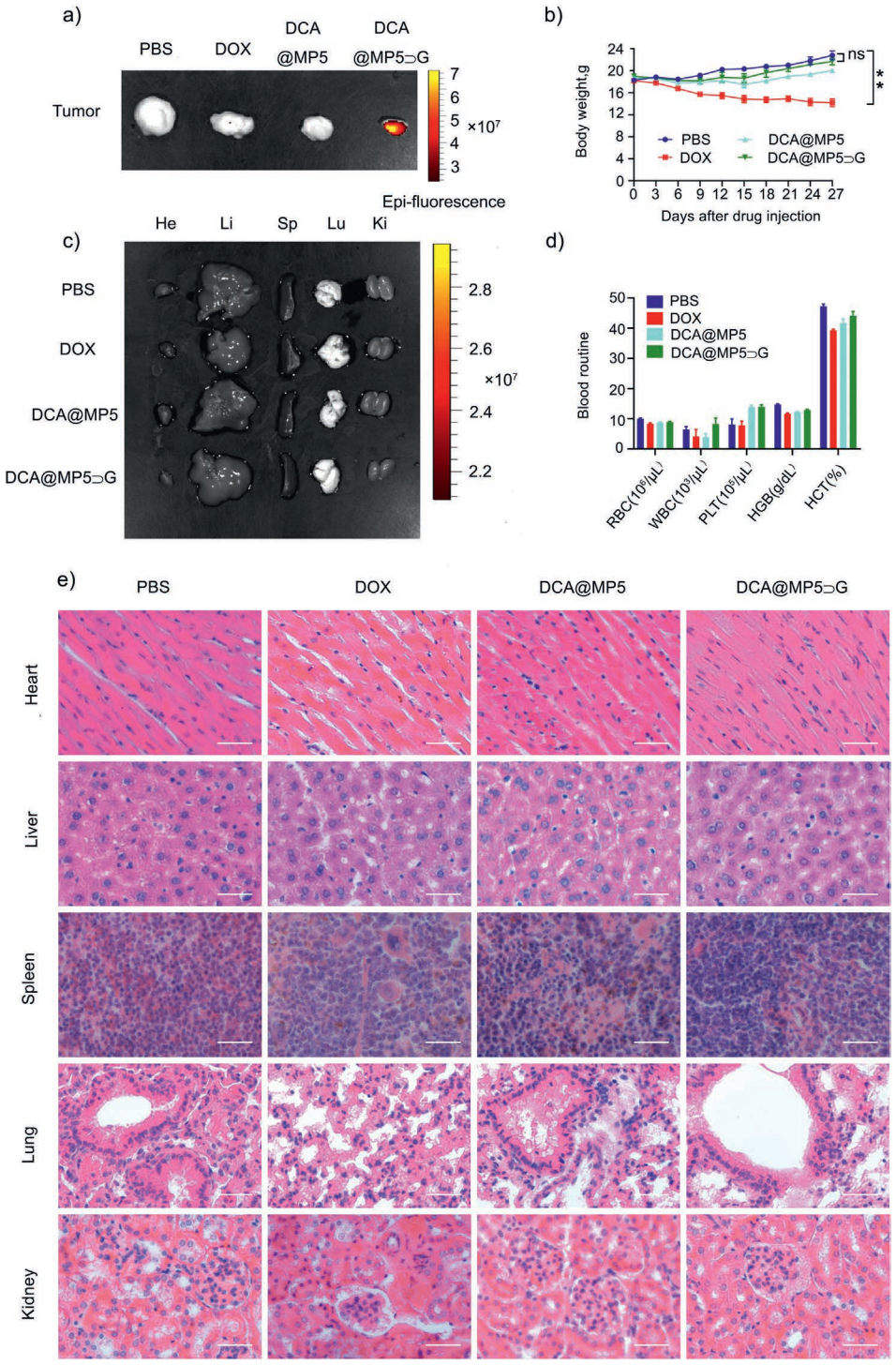


Fig. 6. *In vivo* fluorescence imaging of HepG2 subcutaneous tumor-bearing BALB/c nude mice after intravenous injection of different formulations. (a) Fluorescence detection in tumors. (b) Fluorescence detection in organs (heart, liver, spleen, lung and kidney). (c) Body weight of mice. (d) Routine blood examination. (e) Histological examination of different organs. Paraffin section thickness: 5 μm; Scale bar: 50 μm. Data are expressed as the mean ± SD ($n = 5$). $^{**}P < 0.001$.

at two-day intervals for 24 consecutive days, then, the mice were euthanized, and the tumor was removed surgically, photographed, and the tumor size was compared. As shown in Figs. 7a and b, treatment with DCA@MP5⊃G in HepG2-bearing BALB/c nude mice led to a notable reduction in tumor size and tumor volume. Moreover, the tumor weight in the DCA@MP5⊃G group was significantly lower compared to the group without galactose targeting, demonstrating that DOX-loaded DCA@MP5⊃G exhibits the most potent anti-tumor efficacy (Fig. 7c). In addition, tumor tissues from the tumor-bearing nude mice were dissected following the treatment cycle and subjected to HE staining to evaluate the destructive effect of the DOX-loaded DCA@MP5⊃G nano drug delivery system on tumor tissues. As shown in Fig. 7d, the histological structure of tumor tissues treated with DOX-loaded DCA@MP5⊃G exhibited severe damage, characterized by loosened tumor tissues and reduced tumor cell density. In addition, we conducted a terminal deoxynucleotidyl transferase dUTP nick end labeling (TUNEL) assay to evaluate tumor tissue cell apoptosis and performed Ki67

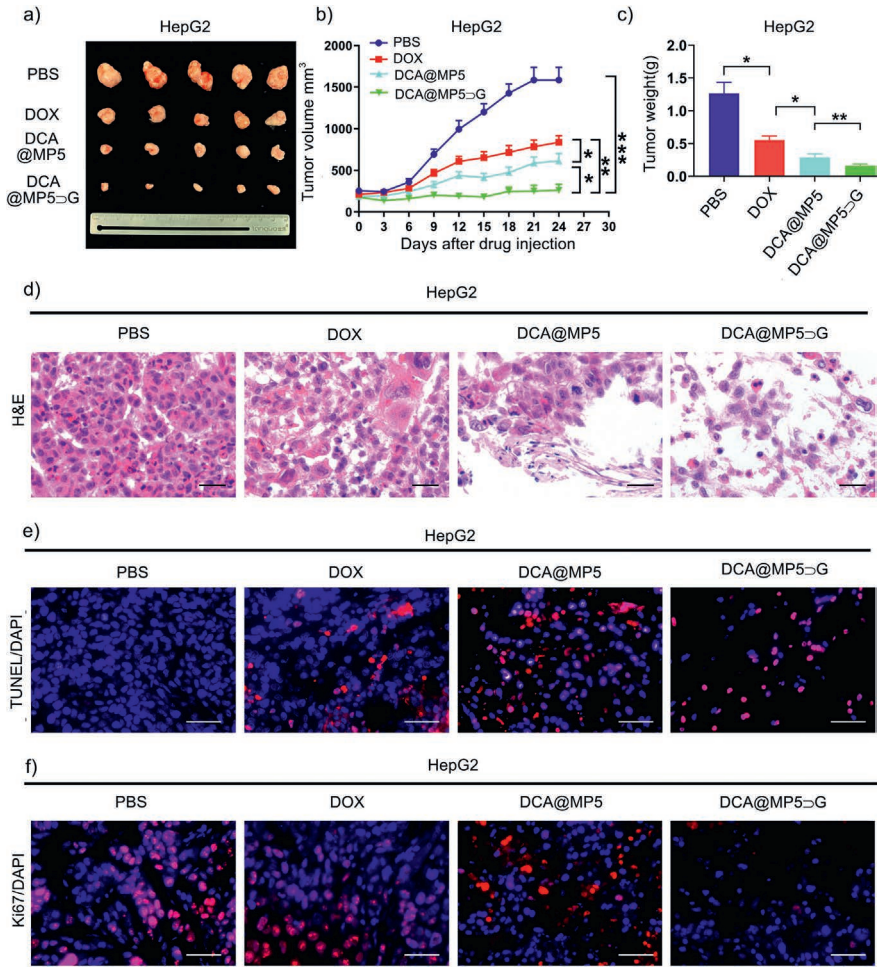


Fig. 7. Therapeutic efficacy of chemo drugs in HepG2 tumor bearing BALB/C nude mice treated with various intravenous administrations: (a) Tumor morphology; (b) Tumor volume; (c) Tumor weight; (d) Histology of tumor; (e) TUNEL assay; and (f) Ki67 staining. Paraffin section thickness: 5 μm; Scale bar: 50 μm. All data are mean ± SD, $n = 5$, $^{*}P < 0.05$, $^{**}P < 0.001$.

immunofluorescence staining to assess tumor cell proliferation. As shown in Fig. 7e, the TUNEL assay revealed that DCA@MP5⊃G significantly induced irreversible apoptosis in a substantial number of tumor cells. Furthermore, the proportion of Ki67-positive cells in tumor tissues of the DCA@MP5⊃G group was the lowest, whereas higher proportions of Ki67-positive cells were observed in the control groups (Fig. 7f). All aforementioned results showed that our DCA@MP5⊃ G nano platform facilitates the delivery of DOX to tumors, severely destroyed the histological structure of tumor cells, effectively induced tumor cell apoptosis and inhibited tumor cell proliferation, thereby enhancing therapeutic outcomes, reducing side toxicity and providing a new means for cancer therapy.

In this work, based on the specific interaction between carbohydrates and proteins and the extensive multifunctional integration ability of the supramolecular system, we successfully developed a novel "dual sweet" supramolecular hybrid nanocarrier CA@MP5⊃G with pH responsiveness and tumor-targeting ability for efficient targeted delivery of anticancer drug. The research results show that this system can efficiently load the anticancer drug DOX. Through the interaction between the guest molecule galactose derivative and the overexpressed ASGPR on the surface of HepG2 cells, it can mediate the targeting of nanoparticles to hepatocellular carcinoma cells. The *in vitro* drug release simulation results indicate that the acid-sensitive supramolecular hybrid nanomaterial composed of Con A and mannosyl pillararene has a good ability to release drug in response to stimuli in a simulated low pH tumor environment. Meanwhile, this system has an excellent killing effect on cancer cells and can effectively reduce the toxicity of DOX to normal cells. The results of *in vivo* experiments on mice also prove that this system has good tumor-targeting properties and can effectively inhibit tumor growth. This design provides a theoretical basis for the application of drug delivery systems based on the specific interaction between carbohydrates and proteins in anti-tumor therapy. This will be a fruitful exploration in the field of supramolecular hybrid nanomaterials and also provides an excellent example for the development of high-efficiency biomedicines.

Declaration of competing interest

The authors declare that they have no known competing financial interests or personal relationships that could have appeared to influence the work reported in this paper.

CRediT authorship contribution statement

Kun Shang: Visualization, Methodology, Formal analysis, Data curation, Conceptualization. **Yinghua Lv:** Writing – original draft, Visualization, Methodology, Formal analysis, Data curation. **Yibo Yang:** Writing – original draft, Visualization, Methodology, Formal analysis. **Senyu Yang:** Visualization, Methodology, Formal analysis, Data curation. **Zelong Chen:** Methodology, Data curation. **Ke Yang:**

Methodology, Data curation. **Cong Li:** Methodology, Formal analysis. **Shuang Chao:** Writing – original draft, Visualization, Project administration, Funding acquisition, Formal analysis. **Yuchao Lu:** Writing – original draft, Methodology, Funding acquisition, Data curation. **Yuxin Pei:** Writing – review & editing, Project administration, Funding acquisition. **Zhichao Pei:** Writing – review & editing, Writing – original draft, Project administration, Funding acquisition.

Acknowledgments

This work was supported by the National Natural Science Foundation of China (Nos. 22577103, 22571257, 22301246), and the Project of Science and Technology of Social Development in Shaanxi Province (Nos. 2023-YBSF-151, 2024SF-YBXM-294), and the Shaanxi Province Postdoctoral Science Foundation (No. 2023BSHEDZZ101), the Fundamental Research Program of Shanxi Province (No. 202403021221212), and the Research Foundation Project of Changzhi Medical College (No. HZZD202406). The authors thank the Teaching and Research Core Facility at College of Life Science (Ningjuan Fan), Life Science Research Core Services (Kerang Huang, Min Zhou), and Crop Biology Innovation Center, Northwest A&F University, for characterizations.

Supplementary materials

Supplementary material associated with this article can be found, in the online version, at doi:10.1016/j.cclet.2025.111798.

References

[1] S. Chagri, D.Y.W. Ng, T. Weil, Nat. Rev. Chem. 6 (2022) 320–338.
[2] C.G. Palivan, R. Goers, A. Najer, et al., Chem. Soc. Rev. 45 (2016) 377–411.
[3] C. Liu, H. Ma, S. Yuan, Y. Jin, W. Tian, ACS Nano 19 (2025) 2047–2069.
[4] M. Delbianco, P. Bharate, S. Varela-Aramburu, P.H. Seeberger, Chem. Rev. 116 (2016) 1693–1752.
[5] S. Zhang, K.Y. Chen, X. Zou, Commun. Inf. Syst. 21 (2021) 147–163.
[6] Y. Wang, Z. Chen, J. Li, et al., Adv. Sci. 11 (2024) 2306178.
[7] W. Feng, Y. Lv, Z. Chen, et al., Chem. Eng. J. 417 (2021) 129178.
[8] S. Bassagañas, S. Carvalho, A.M. Dias, et al., PLoS One 9 (2014) 14.
[9] Y. Lin, D.M. Lubman, Acta Pharm. Sin. B 14 (2024) 1098–1110.
[10] J.Y. Zhou, B.A. Cobb, Annu. Rev. Immunol. 39 (2021) 511–536.
[11] J. Li, Z. Chen, Z. Pei, Y. Pei, Chem. Eng. J. 507 (2025) 159884.
[12] C. Gao, G. Chen, Acc. Chem. Res. 53 (2020) 740–751.
[13] G. Yang, X. Zhang, Z. Kochovski, et al., J. Am. Chem. Soc. 138 (2016) 1932–1937.
[14] L. Su, W. Zhang, X. Wu, et al., Small 11 (2015) 4191–4200.
[15] G. Yang, H.M. Ding, Z. Kochovski, et al., Angew. Chem. Int. Ed. 56 (2017) 10691–10695.
[16] S.H. Kim, C.H. Kim, C.H. Lee, et al., Biomaterials 318 (2025) 123165.
[17] J. Li, Y. Li, Y. Wang, et al., Chem. Eng. J. 505 (2025) 159201.
[18] J. Liu, Z. Sun, Y. Yuan, et al., ACS Appl. Mater. Interfaces 8 (2016) 6917–6924.
[19] G. Ada, D. Isaacs, Clin. Microbiol. Infec. 9 (2003) 79–85.
[20] Z. Li, L. Gu, J. Agric. Food. Chem. 62 (2014) 1301–1309.
[21] J. Feng, S. Wu, H. Wang, S. Liu, J. Funct. Foods 27 (2016) 55–68.
[22] F. Yin, J.J. Li, B. Shi, et al., Mater. Chem. Front. 7 (2023) 5263–5287.
[23] S. Chao, P. Huang, Z. Shen, et al., Org. Chem. Front. 10 (2023) 3491–3497.
[24] Y. Song, Y. Chen, P. Li, C.M. Dong, Biomacromolecules 21 (2020) 5345–5357.
[25] Y. Liu, Y. Zhang, Z. Wang, et al., J. Am. Chem. Soc. 138 (2016) 12387–12394.
[26] N. Jayaraman, Chem. Soc. Rev. 38 (2009) 3463–3483.
[27] L. Wu, Y. Zhang, Z. Li, et al., J. Am. Chem. Soc. 139 (2017) 14684–14692.
[28] Y.H. Song, Q. Bian, F. Wang, et al., Coord. Chem. Rev. 524 (2025) 216299.
[29] Z. Li, Z. Shen, Y. Pei, S. Chao, Z. Pei, Chem. Commun. 59 (2023) 989–1005.
[30] K. Kato, S. Fa, S. Ohtani, et al., Chem. Soc. Rev. 51 (2022) 3648–3687.
[31] M.J. Webber, R. Langer, Chem. Soc. Rev. 46 (2017) 6600–6620.
[32] Y. Chang, K. Yang, P. Wei, et al., Angew. Chem. Int. Ed. 53 (2014) 13126–13130.
[33] K. Yang, Y. Chang, J. Wen, et al., Chem. Mater. 28 (2016) 1990–1993.
[34] T. Ogoshi, S. Kanai, S. Fujinami, T.A. Yamagishi, Y. Nakamoto, J. Am. Chem. Soc. 130 (2008) 5022–5023.
[35] H. Zeng, P. Liu, H. Xing, F. Huang, Angew. Chem. Int. Ed. 61 (2022) e202115823.
[36] J. Li, B. Hu, Z. Chen, et al., Chem. Sci. 15 (2024) 765–777.
[37] K. Wang, R. Zhang, Z. Song, et al., Adv. Sci. 10 (2023) 2206897.
[38] S. Chao, Z. Shen, Y. Pei, et al., Chem. Commun. 57 (2021) 7625–7628.
[39] K. Buffet, I. Nierengarten, N. Galanos, et al., Chem. Eur. J. 22 (2016) 2955–2963.
[40] Z. Liu, F. Demontrond, A. Imberty, et al., Chin. Chem. Lett. 34 (2023) 107872.
[41] X. Chen, Y. Yang, Q. Mai, et al., Biomaterials 304 (2024) 122384.
[42] N. Galanos, E. Gillon, A. Imberty, S.E. Matthews, S. Vidal, Org. Biomol. Chem. 14 (2016) 3476–3481.
[43] T.Mohy El Dine, R. Jimmidi, A. Diaconu, et al., J. Med. Chem. 64 (2021) 14728–14744.
[44] G. Yu, Y. Ma, C. Han, et al., J. Am. Chem. Soc. 135 (2013) 10310–10313.
[45] F. Chen, S. Goel, H.F. Valdovinos, et al., ACS Nano 9 (2015) 7950–7959.
[46] Y. Qin, N. Niu, X. Li, et al., Aggregate 6 (2025) e708.